

Surface Plasmon-Enhanced Nano-photodetector for Green Light Detection

Lin-Bao Luo¹ · Kun Zheng¹ · Cai-Wang Ge¹ · Yi-Feng Zou¹ · Rui Lu¹ · Yuan Wang¹ · Dan-Dan Wang¹ · Teng-Fei Zhang¹ · Feng-Xia Liang²

Received: 27 July 2015 / Accepted: 17 September 2015
© Springer Science+Business Media New York 2015

Abstract Light manipulation is vitally important for one-dimensional semiconductor nanostructure-based photodetectors which have great potential in future optoelectronic circuits, imaging technique, and light-wave communication. In this paper, we reported a plasmonic gold nanoparticle (AuNP)-decorated nano-photodetector for green light sensing. It is found that the as-fabricated device exhibits obvious increase in light absorption in the range from 400 to 550 nm, after functionalization of plasmonic AuNPs. Further device performance analysis reveals that the photocurrent of the plasmonic photodetector was increased by more than sevenfold, compared with that without coating. What is more, both responsivity and detectivity are found to increase as well. According to theoretical simulation based on the finite element method (FEM), the observed enhancement in device performance can be attributed to the surface plasmon-induced direct electron injection from the metal nanoparticles to the semiconductor nanostructures.

Keywords II-VI group semiconductors · Surface plasmon · Electron injection · Photoresponsivity · FEM

✉ Lin-Bao Luo
luolb@hfut.edu.cn

✉ Feng-Xia Liang
fxliang@hfut.edu.cn

¹ School of Electronic Sciences and Applied Physics, Hefei University of Technology, Hefei, Anhui 230009, People's Republic of China

² School of Materials Science and Engineering and Anhui Provincial Key Laboratory of Advanced Functional Materials and Devices, Hefei University of Technology, Hefei, Anhui 230009, People's Republic of China

Introduction

Surface plasmon resonance (SPR), as we know, is the charge-density oscillation that may exist at the interfaces of two media with opposite dielectric constants, for example, a dielectric and a metal [1]. Localized SPR (LSPR) effect, usually associated with noble metal nanostructures (e.g., gold nanoparticles, silver nanoparticles), creates sharp spectral absorption and scattering as well as strong localized field enhancement. The past two decades have witnessed great progresses in the synthesis of plasmonic noble metal nanoparticles for biological sensors and photocatalysis application, since the first discovery of SPR-based gas detection and biosensors by Nylander and Liedberg [2, 3]. LSPR effect has proved to be a highly reliable and efficient sensing strategy that can provide a non-invasive, label-free means of detection in real time [4, 5]. In addition, LSPR effect has also been utilized as an approach to localize incident light at nanoscale level for improving light confinement when designing high-performance optoelectronic device [6, 7], such as photovoltaic devices [8–10], light emitting diode (LEDs) [11, 12], photodetector [13–15], optical waveguide [16, 17], electrochromic devices [18], and thermoelectric devices [19, 20].

Zinc telluride (ZnTe), with a moderate and direct band gap of 2.3 eV, is one of the most important II-VI semiconductor compounds [21]. Due to their unique electrical and optical properties, one-dimensional (1-D) ZnTe nanostructures have displayed great potential for blue photodetection, which is vitally important to space communication and future complicated optoelectronic circuits [22, 23]. For example, Cao et al. reported on a blue green light photodetector based on single-crystal ZnTe nanowires (ZnTeNWs). It was found that the device exhibited obvious sensitivity to 500-nm light illumination with photoconductive gain of 1.5×10^4 [24]. What is more, Wu et al. developed a nano-photodetector based on

Sb-doped ZnTe nanoribbon with *p*-type conductivity [25]. They found that the nano-photodetector based on ZnTe:Sb/Si heterojunction has a responsivity of 1.8×10^3 and photoconductive gain of 4.2×10^3 , respectively. In spite of these efforts, the performance of these ZnTeNW-based green detectors is still limited by low responsivity and quantum efficiency, which is mainly due to the relatively small photon absorption cross section [26]. In view of the light confinement of LSPR effect mentioned above, we herein report a plasmonic green light nano-photodetector. Owing to the coexistence of surface plasmon band of the gold nanoparticles (AuNPs) and the band gap of the semiconductor nanostructures, the absorption cross sections of ZnTeNWs was clearly increased in the sensitivity region. Both experimental absorption and theoretical simulation based on the finite element method (FEM) shows that the plasmonic AuNPs are capable of trapping incident light through LSPR effect, which is highly beneficial to the detection of green light illumination. Further device analysis reveals that the responsivity, gain, and detectivity of the plasmonic nano-photodetector were pronouncedly enhanced after the coating of AuNPs. The generality of this study demonstrated that LSPR is an effective strategy to increase the device performance of one-dimensional semiconductor nanostructure-based optoelectronics.

Result and Discussion

The proof-of-concept plasmonic nanodevice was assembled by a widely used photolithography method, in which the electrodes were defined by photolithography, followed by e-beam deposition and lift-off [27, 28]. As schematically shown in Fig. 1a, the plasmonic green light nano-photodetector was

composed of two parallel metal electrodes, bridged by individual ZnTeNW whose surface was functionalized with many plasmonic AuNPs. The thickness of the Cu/Au electrode is about 2/48 nm. In this study, the ZnTeNWs were synthesized by a thermal evaporation method (see the “Experimental Section”). According to the scanning electron microscope (SEM) image shown in Fig. 1b, the NWs are about tens of micrometers in length and 400–600 nm in diameter. Moreover, the ZnTeNWs have smooth surface and uniform diameter along the growth direction. After reaction with HAuCl₄ at 120 °C under hydrothermal condition for 1 h, the NW surface becomes rather rough (Fig. 1c). Figure 1d shows the X-ray diffraction (XRD) pattern of these nanostructures. All the peaks can be readily ascribed to *fcc* Au and hexagonal ZnTe (JCPDS card no. 15.0746) [29]. Further energy-dispersive X-ray spectroscopy (EDS) analysis in Fig. 1e confirms that the nanostructure is composed of three elements, e.g., Zn, Te, and Au. In fact, the coating of AuNPs was also confirmed by further XPS analysis. As shown in Fig. 1f, two peaks at 87.6 and 83.7 eV in the Au 4f spectrum can be attributed to Au in the form of 0 valence [30]. Understandably, the AuNPs on the surface ZnTe NW were formed by the following chemical equation: $\text{CH}_3\text{CH}_2\text{OH} + \text{HClCl}_4 \rightarrow \text{AuNPs}$.

To further study the microstructure of the AuNPs@ZnTeNWs, transmission electron microscope (TEM) analysis was analyzed. As shown in Fig. 2a, b, the surface of ZnTeNW becomes much rougher after surface modification. In addition, owing to the distinct difference of Au and ZnTe in contrast, the gold nanoparticles can be readily distinguished from the nanostructure. From the high-resolution transmission electron microscope (HRTEM) images in Fig. 2c–d, one can see clearly that both the AuNPs and ZnTeNW are of single crystal. The elemental mappings of the constituting elements were shown in Fig. 2e–f, in which all the Zn, Te, and Au are uniformly distributed in the NW.

Fig. 1 **a** Schematic illustration of the plasmonic green light nano-photodetector based on individual AuNPs@ZnTeNWs. **b** SEM image of pure ZnTeNWs, *inset* shows a SEM image of the pure ZnTeNWs at large magnification. **c** SEM image of the AuNPs@ZnTeNWs. **d** XRD pattern of the AuNPs@ZnTeNWs. **e** The corresponding EDS spectrum. **f** XPS spectrum of the AuNP-modified ZnTeNWs

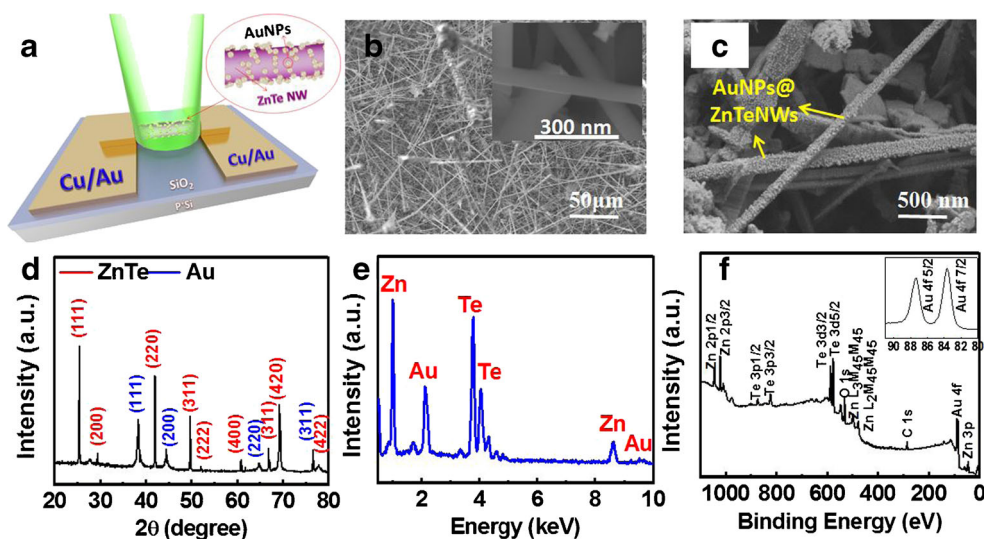
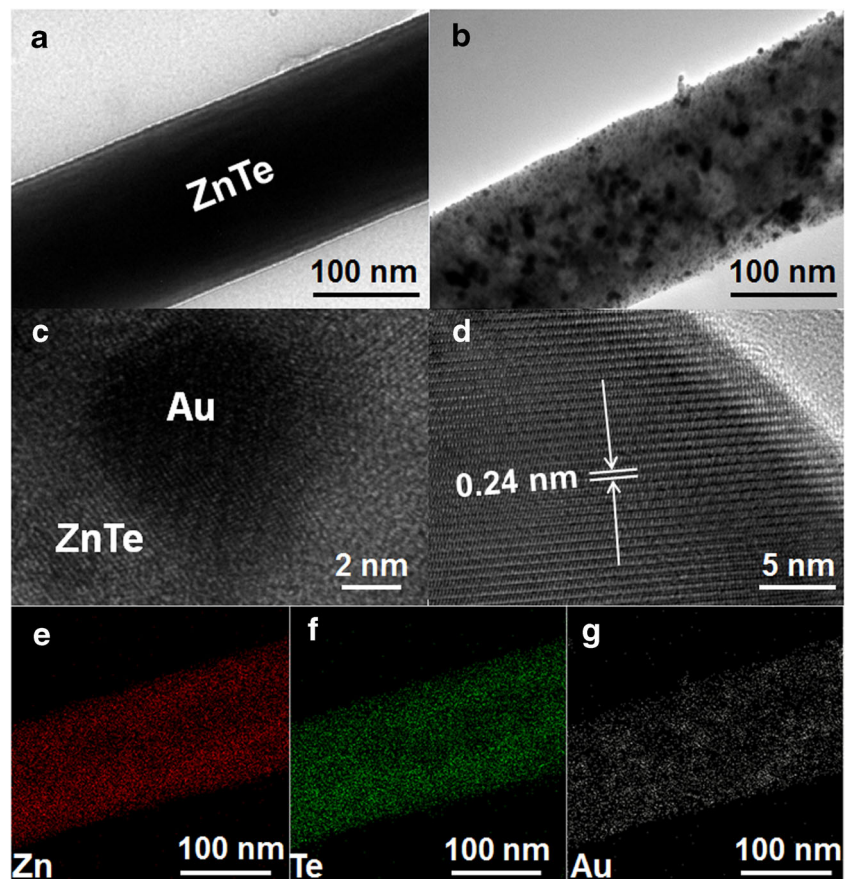


Fig. 2 TEM image of intrinsic **a** ZnTeNW and **b** AuNP-coated ZnTeNW. **c–d** HRTEM images of the AuNP-coated ZnTeNW. **d** HRTEM image of an AuNP. **e** Zn, **f** Te, and **g** Au elemental mapping of a single AuNP-coated ZnTeNW



Notably, due to relatively low concentration, the mapping profile of Au is much vaguer, in comparison with that of both Zn and Te elements.

According to the statistical distribution of the AuNPs shown in Fig. 3a, the diameters of the plasmonic nanoparticles are in the range of 5–25 nm, with an average value of ~15 nm. When shined by light illumination, these AuNPs exhibit typical light absorption at ~500 nm which can be readily ascribed to the LSPR band [31, 32]. To study the diameter-dependent optical property of the plasmonic AuNPs, theoretical simulation based on finite element method (FEM) was carried out. Figure 3b plots the absorption of AuNPs with diameters of 5, 10, 15, 20, and 25 nm, and it is obvious that when the diameter of the NPs is gradually increased from 5 to 25 nm, the intensity of absorption will increase accordingly. What is more, when these AuNPs were modified on the surface of ZnTe NWs, obvious enhancement in electric field was observed at the metal-semiconductor interface (Fig. 3c). Figure 3e display the experimental absorption spectrum of both intrinsic ZnTeNWs and AuNPs@ZnTeNWs. One can see clearly that due to the light trapping effect of the plasmonic AuNPs, the absorption spectrum of the ZnTeNWs was increased in the regime of 400–550 nm after functionalization of AuNPs on the surface of

ZnTeNWs. This result is in rough agreement with the theoretical simulation shown in Fig. 3f.

It should be noted that the enhancement in electric field is highly dependent on the wavelength of light irradiation, as well as the diameter of the AuNPs. Figure 4 illustrate a panel of near-field electric field intensity distribution of AuNPs with diameters of 5, 15, and 25 nm when illuminated by incident light with wavelengths of 400, 520, and 730 nm. It is revealed that compared with AuNPs of smaller diameter (5 and 15 nm), the 25-nm AuNPs can induce a relatively high enhancement in electric field. In addition, the area of hot spots with high electric field energy density under light illumination with 520 nm is larger than that under 400 and 730 nm, in agreement with the plasmon band of AuNPs.

Next, the I - V characteristics of ZnTeNW devices with and without AuNPs were studied in order to unveil the effect of AuNPs on the optoelectronic properties. Figure 5a, b shows the I - V curves of both nanostructure in the dark and under light illumination. The current of both devices is observed to increase linearly with increasing bias voltage, suggesting that ohmic contact was formed between the nanostructures and Cu/Au electrodes. Upon light illumination, both devices exhibit remarkable photocurrent with green light illumination (wavelength 532 nm). Figure 5c shows the photoresponse of

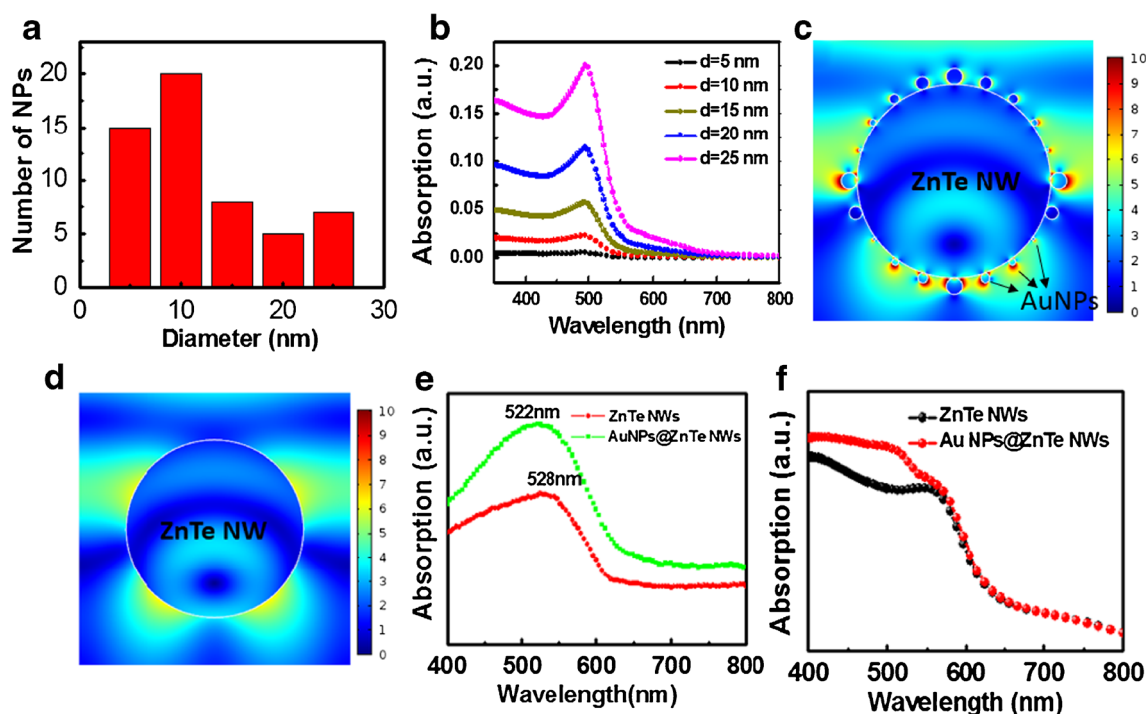


Fig. 3 **a** Diameter distribution of the AuNPs. **b** Theoretical simulation of the AuNPs with different diameters. **c** The electric field distribution $|E|^2$ at the cross section of AuNPs. **d** The electric field distribution $|E|^2$ of pure

ZnTe NW. **e** Experimental absorption spectrum of both intrinsic ZnTeNWs and AuNPs@ZnTeNWs. **f** Theoretical absorption spectrum of both intrinsic ZnTe NWs and AuNPs@ZnTeNWs

both devices at bias voltage of 4 V when the green light illumination was switched on and off alternatively. One can see clearly that both devices can be reversibly switched between high and low resistance states, with excellent reproducibility and stability. Notably, the dark current is slightly increased from 0.96 to 1.42 nA due to the charge transfer as a result of difference in work function [15, 33]. What is more, the photocurrent for AuNPs@ZnTeNW is increased by sevenfold

from 17.7 to 142 nA, yielding an increase of on/off ratio from 18.4 to 98.6. To quantitatively evaluate the influence of plasmonic nanoparticles on the device performance of green light nano-photodetector, the responsivity, gain, and detectivity that reflect the photodetector sensitivity to incident light were calculated by using the following equations [34, 35]:

$$R = \left(\frac{I_p}{P_{\text{opt}}} \right) \quad (1)$$

$$G = R \left(\frac{hc}{q\lambda} \right) \frac{1}{\eta} \quad (2)$$

$$D^* = \frac{1}{\text{NEP}} \approx \sqrt{\frac{A}{2qI_d}} R \quad (3)$$

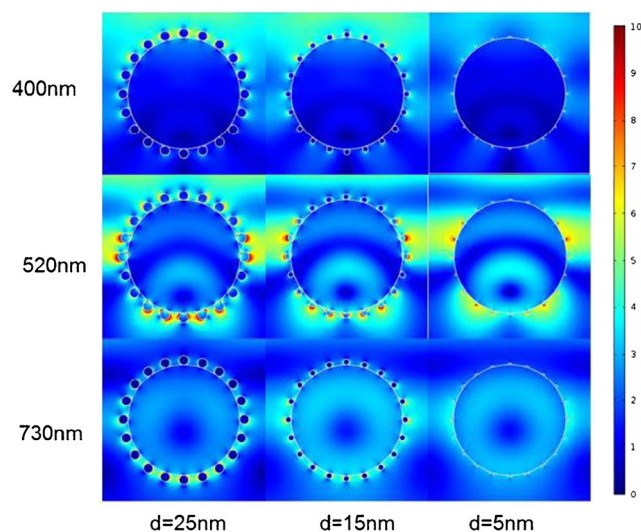
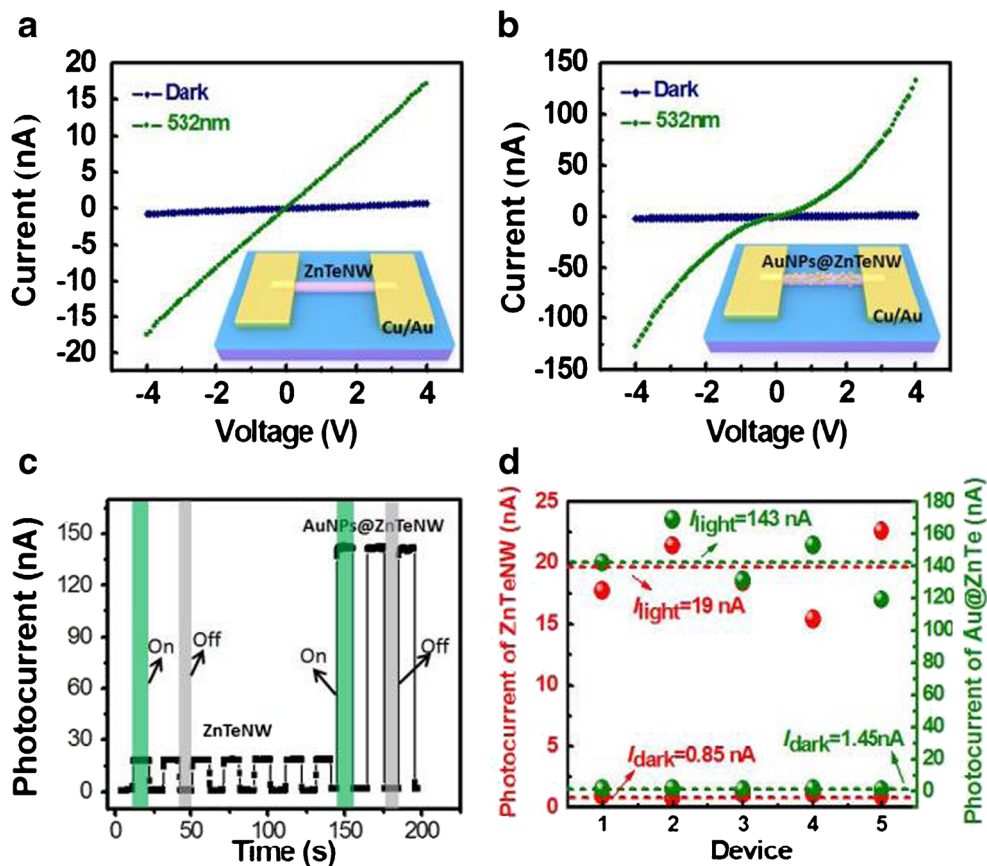


Fig. 4 Simulated electric field energy density distribution of AuNPs with different diameters, the wavelengths of the light are 300, 520, and 710 nm, respectively

where I_p is the photocurrent, P_{opt} the incident light power, q the elementary charge, λ the incident light wavelength, h the Planck's constant, c the light speed, η the quantum efficiency, A the active area of the device, and I_d the dark current, respectively. Based on the above equations, R was calculated to be $6.37 \times 10^2 \text{ AW}^{-1}$ for pure ZnTeNW and $5.11 \times 10^3 \text{ AW}^{-1}$ for AuNPs@ZnTeNW, respectively. By assuming $\eta=1$ for simplification, G and D^* were estimated to be 1.49×10^3 and $5.97 \times 10^{12} \text{ cm Hz}^{1/2} \text{ W}^{-1}$ for pure ZnTeNW and 1.19×10^4 and $3.28 \times 10^{13} \text{ cm Hz}^{1/2} \text{ W}^{-1}$ for AuNPs@ZnTeNW, respectively. Figure 5d compares the dark current and photocurrent of five representative devices before and after AuNPs coating, with four straight lines indicating the average I_{dark} (pure

Fig. 5 **a, b** I - V curve of intrinsic ZnTeNWs and AuNPs@ZnTeNW-based devices in the dark and under 532-nm light illumination, respectively. The insets are the schematic illustration of the device configuration. **c** Photoresponse of ZnTeNWs and AuNPs@ZnTeNW-based devices under repeatable light illumination. **d** The photocurrent and dark current of five representative ZnTeNW and AuNPs@ZnTeNW-based nanophotodetectors



ZnTeNW), I_{light} (pure ZnTeNW), I_{dark} (AuNPs@ZnTeNW), and I_{dark} (AuNPs@ZnTeNW) of 0.85, 19, 1.45, and 143 nA, respectively. Table 1 summarizes the key metrics of the present plasmonic photodetector and other devices based on ZnTe nanostructures. One can see clearly that the responsivity, gain, and detectivity of the AuNPs@ZnTeNW device are higher not only than those of the device made of pure ZnTeNW but also than other ZnTe nanostructure-based green light photodetectors, suggesting that the coating of plasmonic nanoparticles is an efficient strategy to optimize the device performance of one-dimensional nanostructure-based photodetectors. As we will discuss later, such an enhancement in device performance can be attributed to the surface plasmon-induced electron injection from the metal to semiconductor.

The observed optimization in device performance can be attributed to the direct electron transfer from the AuNPs to

ZnTeNW. Figure 6a illustrates the schematic diagram of the plasmonic nanostructures. When shined by light irradiation, the energetic hot electrons from the AuNPs can couple the resonance photo energy and then transfer to the conduction band of ZnTeNWs. Such a charge transfer process (or direct electron transfer, DET) is highly spontaneous because the energy of the hot electrons is as high as 1–4 eV, according to a previous study [36]. As a matter of fact, this DET process is partially verified by separate absorption of both AuNPs and ZnTe. Although the overall absorption of the AuNPs@ZnTeNW is obviously improved in comparison with that of pure ZnTeNW (Fig. 3d), the absorption of sole ZnTe is actually decreased, which is ascribed to the shading effect of the plasmonic AuNPs (Fig. 6b). For the AuNPs@ZnTeNW, the increase in photocurrent should be attributed to LSPR-induced DET, without which the photocurrent should be

Table 1 Comparison of the device performance of the present plasmonic photodetector and other ZnTe nanostructures with similar device configuration

Materials	R (AW^{-1})	G	D^* ($\text{cm Hz}^{1/2} \text{W}^{-1}$)	Reference
ZnTeNW	6.37×10^2	1.49×10^3	5.97×10^{12}	This work
AuNPs@ZnTeNW	5.11×10^3	1.19×10^4	3.28×10^{13}	This work
ZnTeNW	2.2×10^3	1.5×10^3	1.71×10^{11}	[25]
nTeNR/Si	1.8×10^3	4.2×10^3	10^{12}	[26]

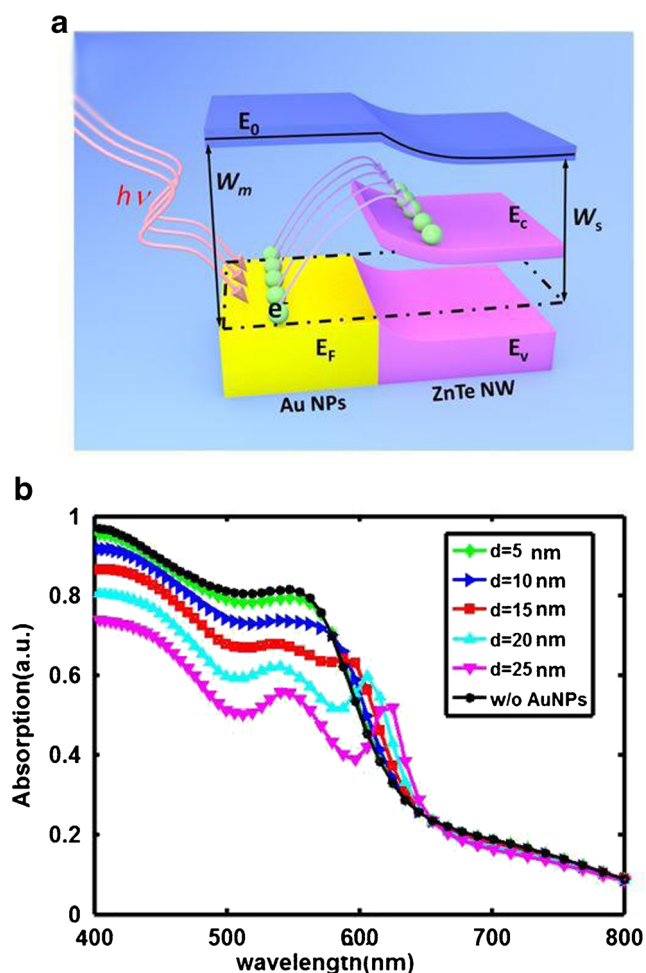


Fig. 6 **a** Schematic illustration of the direct hot electron injection induced by LSPR. **b** Separate theoretical simulation of the absorption of ZnTeNW, the ZnTeNW is coated with AuNPs on its surface

theoretically lower than that of pure ZnTeNW considering the decrease in photoabsorption.

Conclusion

In summary, we have developed a plasmonic nanophotodetector for the detection of green light illumination. Both experimental and theoretical results reveal that the light absorption of the device in the range from 400 to 550 nm was considerably improved after the coating of AuNPs on the surface of ZnTeNW. Optoelectronic analysis the photocurrent of AuNPs@ZnTeNW device was increased by sevenfold, in comparison with that without plasmonic AuNPs. What is more, the responsivity, gain, and detectivity of the plasmonic device were observed to increase substantially after functionalization of AuNPs. Further theoretical simulation suggests that the enhancement of device performance can be attributed to the LSPR-induced DET from metal and semiconductor.

Experimental Section

The Synthesis of the ZnTeNWs and AuNPs@ZnTeNWs In this study, a horizontal tube furnace with two temperature zones was employed to synthesize the ZnTeNWs. Briefly, an Al₂O₃ boat with 0.6-g ZnTe powder (analytical grade, Aladdin Co.) was put into the central position of the furnace. Silicon substrates pre-coated with a layer of 5-nm Au as catalysts were then placed in the downstream position from the precursor (~20 cm). The ZnTe powder was then heated up to 1050 °C at a rate of 30 °C/min, until the tube was evacuated to a base pressure of 10⁻³ Torr. The temperature of the tube will be maintained at 1050 °C for 2 h, during which a carrier gas of high-purity argon premixed with 5 % hydrogen was fed at a total flow rate of 20 standard-state cubic centimeter per minute (Sccm). The product was collected from the Si wafer after the tube was allowed to cool to room temperature. To synthesize AuNPs@ZnTeNWs, 50 mg of as-synthesized ZnTeNWs was added into 20-ml alcohol. A total of 0.15 ml of HClAu₄ solution (0.1 mol/l) was then added into the above solution under vigorous stirring. The result solution was then transferred and sealed in a 30-ml Teflon-lined autoclave, which was kept at 120 °C for 1 h. After reaction, the as-prepared floccule was filtered and rinsed with distilled water and absolute alcohol to remove possible ions and remnants. The phase, morphology, and crystallinity of the ZnTeNWs were studied by X-ray diffractometer (XRD, Rigaku A/Max-γB with Cu Kα radiation), field-emission scanning electron microscope (FESEM, SIRION 200 FEG), and high-resolution transmission electron microscope (HRTEM, JEOL JEM-2010, operating at 200 kV), attached with a selected-area electron diffraction (SAED). The chemical composition of the product was analyzed by X-ray photoelectron spectroscopy (XPS), which is equipped with a monochromatic Al X-ray (1486.6 eV) source.

The Fabrication and Analysis of the Plasmonic Photodetector

The AuNP-coated ZnTeNW photodetector was fabricated by firstly dispersing the nanostructures on Si substrate with 300-nm thick thermally oxidized SiO₂ layer, which was washed stepwise with absolute alcohol and distilled water under ultrasonication for 5 min, respectively. Then the SiO₂/Si substrate containing AuNPs@ZnTeNWs with desired density was spin coated with photoresist. Two parallel electrodes (Cu/Au, 2/48 nm) as source and drain were then defined by UV photolithography, followed by deposition of metal layer through electron beam evaporator. The remaining photoresist was removed by lift-off using acetone. The optoelectronic characteristics of the plasmonic device were performed at a Keithley 4200 semiconductor

characterization system. During analysis, the incident light used in both experiment and simulation was perpendicular to the device, and the polarization is parallel to the length direction of the NW.

Theoretical Modeling The simulation was done by using the finite element method (FEM). The model consisted of different sizes of AuNPs coated on a 300-nm thick ZnTeNW. The permittivity of Au and ZnTe were obtained from Palik and Filmetrics. The incident light is set to be an x -polarized plane wave of 400–800 nm and propagates along y -axis. The boundary conditions at x , z were perfect electric conductors (PEC) and periodic, respectively. Perfect matched layers (PMLs) were used at the top and bottom of the unit cell to reduce the influence of light reflection.

Acknowledgments This work was supported by the Natural Science Foundation of China (NSFC, 21101051, 21501038, and 61575059), the Fundamental Research Funds for the Central Universities (2012HGCH0003, 2013HGCH0012, 2014HGCH0005), the China Postdoctoral Science Foundation (103471013), and the Natural Science Foundation of Anhui Province (Grant no. J2014AKZR0036).

References

- Homola J (2008) Surface plasmon resonance sensors for detection of chemical and biological species. *Chem Rev* 108(2):462–493
- Nyberg C, Liedberg B, Lind T (1982) Gas detection by means of surface plasmon resonance. *Sensors Actuators* 3(1):79–88
- Liedberg B, Nylander C, Lundstrom I (1983) Surface plasmon resonance for gas detection and biosensing. *Sensors Actuators* 4(2):299–304
- Cottat M et al (2013) Localized surface plasmon resonance (LSPR) biosensor for the protein detection. *Plasmonics* 8:699–704
- Sepulveda B et al (2009) LSPR-based nanobiosensors. *Nano Today* 4(3):244–251
- Luo LB et al (2014) Light trapping and surface plasmon enhanced high-performance NIR photodetector. *Sci Rep* 4:3914
- Beck FJ, Lasanta T, Konstantatos G (2014) Plasmonic Schottky nanojunctions for tailoring the photogeneration profile in thin film solar cells. *Adv Opt Mater* 2(5):493–500
- Atwater HA, Polman A (2010) Plasmonics for improved photovoltaic devices. *Nat Mater* 9(3):205–213
- Tan HR et al (2012) Plasmonic light trapping in thin-film silicon solar cells with improved self-assembled silver nanoparticles. *Nano Lett* 12(8):4070–4076
- Xie C et al (2014) Core-shell heterojunction of silicon nanowire arrays and carbon quantum dots for photovoltaic devices and self-driven photodetectors. *ACS Nano* 8(4):4015–4022
- Okamoto K et al (2004) Surface-plasmon-enhanced light emitters based on InGaN quantum wells. *Nat Mater* 3(9):601–605
- Kock A et al (1990) Strongly directional emission from AlGaAs/GaAs light-emitting diodes. *Appl Phys Lett* 57(22):2327
- Berini P (2014) Surface plasmon photodetectors and their applications. *Laser Photonics Rev* 8(2):197–220
- Luo LB et al (2014) The effect of plasmonic nanoparticles on the optoelectronic characteristics of CdTe nanowires. *Small* 10(13):2645–2652
- Miao JS et al (2015) High-responsivity graphene/InAs nanowire heterojunction near-infrared photodetectors with distinct photocurrent on/off ratios. *Small* 11(8):936–942
- Oulton RF et al (2010) A hybrid plasmonic waveguide for sub-wavelength confinement and long-range propagation. *Nat Photonics* 2(8):496–500
- Gao X et al (2013) Ultrathin dual-band surface plasmonic polariton waveguide and frequency splitter in microwave frequencies. *Appl Phys Lett* 102(15):151912
- Tsuboi A, Nakamura K, Kobayashi N (2013) A localized surface plasmon resonance-based multicolor electrochromic device with electrochemically size-controlled silver nanoparticles. *Adv Mater* 25(23):3197–3201
- Feng ZY et al (2014) Widely adjustable and quasi-reversible electrochromic device based on core-shell Au-Ag plasmonic nanoparticles. *Adv Opt Mater* 2(12):11741180
- Xiong YJ et al (2012) Solar energy conversion with tunable plasmonic nanostructures for thermoelectric devices. *Nanoscale* 4(15):4416–4420
- Jie JS et al (2010) One-dimensional II-VI nanostructures: synthesis, properties and optoelectronic applications. *Nano Today* 5(4):313–336
- Zeng LH et al (2013) Monolayer graphene/germanium Schottky junction as high-performance self-driven infrared light photodetector. *ACS Appl Mater Interfaces* 5(19):9362–9366
- Wu W, Bonakdar A, Mohseni H (2010) Plasmonic enhanced quantum well infrared photodetector with high detectivity. *Appl Phys Lett* 96(16):161107
- Cao YL et al (2011) Single-crystalline ZnTe nanowires for application as high-performance green/ultraviolet photodetector. *Opt Express* 19(7):6100–6108
- Wu D et al (2012) Device structure-dependent field-effect and photoresponse performances of p-type ZnTe:Sb nanoribbons. *J Mater Chem* 22(13):6206–6212
- Lu JF et al (2015) Improved UV photoresponse of ZnO nanorod arrays by resonant coupling with surface plasmons of Al nanoparticles. *Nanoscale* 7(8):3396–3403
- Lou Z et al (2015) High-performance rigid and flexible ultraviolet photodetectors with single-crystalline ZnGa₂O₄ nanowires. *Nano Res* 8(7):2162–2169
- Li L et al (2010) Ultrahigh-performance solar-blind photodetector based on individual single-crystalline In₂Ge₂O₇ nanobelts. *Adv Mater* 22(45):5145–5149
- Luo LB et al (2015) p-type ZnTe:Ga nanowires: controlled doping and optoelectronic device application. *RSC Adv* 5(18):13324–13330
- Luo LB et al (2014) Surface plasmon resonance enhanced highly efficient planar silicon solar cell. *Nano Energy* 9:112–120
- Kelly KL et al (2003) The optical properties of metal nanoparticles: the influence of size, shape, and dielectric environment. *J Phys Chem B* 107(3):668–677
- Zhang Q et al (2011) A highly active titanium dioxide based visible-light photocatalyst with nonmetal doping and plasmonic metal decoration. *Angew Chem Int Ed* 50(31):7088–7092
- Han N et al (2013) Tunable electronic transport properties of metal-cluster-decorated III-V nanowire transistors. *Adv Mater* 25(32):4445–4451
- Nie B et al (2013) Monolayer graphene film on ZnO nanorod array for high-performance Schottky junction ultraviolet photodetectors. *Small* 9(17):2872–2789
- Wang MZ et al (2013) TiO₂ nanotube array/monolayer graphene film Schottky junction ultraviolet light photodetectors. *Part Part Syst Charact* 30(7):630–636
- Linic S, Christopher P, Ingram DB (2011) Plasmonic-metal nanostructures for efficient conversion of solar to chemical energy. *Nat Mater* 10(12):911–921